Identifying Hidden Li-Si-O Phases for Lithium-Ion Batteries via First-Principles Thermodynamic Calculations

Jiale Qu[a, §], Chao Ning[a, §], Xiang Feng[a], Bonan Yao[a], Bo Liu[b], Ziheng Lu[c], Tianshuai Wang[a], Zhi Wei Seh[d], Siqi Shi[e*], Qianfan Zhang[a*]

[a] *School of Materials Science and Engineering, Beihang University, Beijing 100191, China.*

[b] *College of Mathematics and Physics, Jinggangshan University, Ji'an, Jiangxi 343009, China*

[c] *Department of Materials Science & Metallurgy, University of Cambridge, CB3 0FS, United Kingdom*

[d] *Institute of Materials Research and Engineering, Agency for Science, Technology and Research (A*STAR), Singapore 138634, Singapore.*

[e] *School of Materials Science and Engineering, Shanghai University, Shanghai 200444, China.*

[§] ***Author contributions:*** *These authors contributed equally to this work.*

***Corresponding authors**: qianfan@buaa.edu.cn (Qianfan Zhang); sqshi@shu.edu.cn (Siqi Shi)*

Abstract

Si-O based materials are promising alloying and conversion-type anode materials for lithium-ion batteries and are recently found to be excellent dendrite-proof layers for lithium-metal batteries. However, only a small fraction of the Li-Si-O compositional space has been reported, significantly impeding the understanding of the phase transition mechanisms and the rational design of these materials both as anodes and as protection layers for lithium-metal anodes. Herein, we identify three new thermodynamically stable phases within the Li-Si-O ternary system (Li_2SiO_5, Li_4SiO_6 and Li_4SiO_8) in addition to the existing records via first-principles calculations. The electronic structure simulation shows that Li_2SiO_5 and Li_4SiO_8 phases are metallic in nature, ensuring high electronic conductivity required as electrodes. Moduli

calculations demonstrate that the mechanical strength of Li-Si-O phases is much higher than that of lithium metal. The diffusion barriers of interstitial Li range from 0.1 to 0.6 eV and the interstitial Li hopping serves as the dominating diffusion mechanism in the Li-Si-O ternary systems compared with vacancy diffusion. These findings provide a new strategy for future discovery of improved alloying anodes for lithium-ion batteries and offer important insight towards the understanding of the phase transformation mechanism of alloy-type protection layers on lithium metal anodes.

Keywords: Crystal structure prediction; Anode material; First-principles calculations; Ternary alloy phase

1. Introduction

Owning to the high specific capacity (3860 mAh g^{-1} *vs.* 370 mAh g^{-1} of conventional graphite anodes) and low redox potential (−3.04 V *vs.* standard hydrogen electrode), lithium metal is considered the "holy-grail" anode material for lithium-based rechargeable batteries [1–8]. Unfortunately, issues such as uncontrollable side reactions and dendrite growth during electrochemical cyclic conditions remain unsolved [9–16]. Recently, the application of alloy anodes has been developed to overcome these critical issues. In general, lithium alloys possess high Li ion conductivity and high theoretical capacity which can approach that of lithium metal [17,18]. However, the smart design of alloy anodes can efficiently address dendrite growth of lithium metal during cycling [19]. Lithium alloys such as Li_xM (M = Si, Ge, Al, Sn, etc.) have been researched thoroughly, which display high gravimetric and volumetric capacity due to their high Li packing density and safe thermodynamic potentials

compared to carbonaceous materials like graphite [20–28]. However, alloy phase undergoes a larger volume change during lithium extraction and insertion [29,30], causing pulverization of the metal particles and inducing loss of electrical contact between active material and current collector [20]. Numerous approaches have been studied to solve this problem. Among them, combining some non-lithium elements (such as Co, Ni, C, B, N, S and O) with alloy phase to prepare a ternary alloy [24,28,31-35] can not only maintain the good electrical conductivity, but also endow the original alloys with better mechanical properties to suppress volume expansion. Therefore, the exploration of ternary system electrode materials provides a promising pathway for the development of next-generation electrode materials.

Silicon, due to its good chemical properties and diversity of valence states, can form a variety of high Li-content alloy phases with lithium. Si-based materials can alloy with lithium to give a theoretical capacity of 4200 $mAh \cdot g^{-1}$ ($Li_{22}Si_5$) [36–39], which is the highest capacity of any of the lithium alloys studied to date. However, Li-Si alloy electrodes still face great challenges such as large volume expansion. By introducing oxygen element to form a strong silicon-oxygen bond, the phase transition of silicon can be effectively suppressed during the lithium insertion process. Meanwhile, oxygen can also form high-energy compounds such as Li_2O_2 and increase the theoretical specific energy of lithium batteries [40–43]. Therefore, by introducing silicon and oxygen elements to obtain a Li-Si-O ternary alloy matrix, we can achieve a superior ion conductive system with high lithium content, while the volume expansion can be effectively suppressed during the lithium intercalation process, which has already been

demonstrated by experiment [44]. Therefore, such Li-Si-O ternary system represents a promising anode system that can lead to stable cycling performance.

Typical theoretical studies on alloy anodes lie on the structure identification of alloy phases with various lithium concentrations, which is critical in revealing the phase transition mechanism during the non-ionic chemical reaction process and clarifying the electrochemical properties at different evolution stages. Meanwhile, the environmental factors, such as charging voltage and electrolyte type, can also have a great influence on the composition of anodes. As a result, novel phases, which are not existent in usual conditions, can appear at specified lithation stages or electro-chemical windows. Therefore, evolutionary algorithms and high-throughput methods need to be developed in order to speed up the theoretical simulation. Such structure identification scheme has already been used on lithium battery systems. Hautier *et al.* [45] used high-throughput methods to predict novel mixed polyanions structures ($Li_3MnCO_3PO_4$, $Li_3VCO_3SiO_4$) for lithium-ion battery cathode materials. Through evolutionary algorithms crystal structure prediction techniques, Wang *et al.* [24] identified a new layered oxysulfide LiAlSO in orthorhombic structure as a novel lithium superionic conductor and revealed the remarkable potential of oxysulfides applied as solid electrolytes in lithium batteries. However, most works focus on cathode materials and solid electrolytes, and less studies are done on anode materials. On the other aspect, change of elemental content occurs frequently during the non-ionic reaction process, which needs to be identified [46,47]. For Li-Si-O anodes mentioned above, the internal composition evolution of intermediate alloy phases during the charge/discharge reaction needs to be determined, which is the

prerequisite for investigating the stability, electronic structure and lithium ion diffusivity. However, due to the complexity of ternary compounds, and the variety of valance states for the Si element, many possible phases can stably exist during the lithiation process. Therefore, theoretical simulations with high-throughput screening routines are required to identify this ternary system.

In the present work, crystal structure predictions coupled with first-principles calculations are performed to explore the Li-Si-O ternary system. The rationality and stability of the predicted phases are further verified by Si valence analysis and formation energy analysis. Three previously unidentified thermodynamically stable phases (Li_2SiO_5, Li_4SiO_6 and Li_4SiO_8) are predicted within the Li-Si-O phase diagram, which all display relatively superior dynamic stability. We further analyze the electrochemical windows of these energetically favored phases. These phases are found to exist within the high voltage regime. The calculated moduli are comparable to those of the traditional binary alloy systems from the SPSE database [48], indicating the Li-Si-O ternary alloy electrode exhibits advantages in mechanical strength. Further computations reveal Li interstitial hopping with barriers of 0.1 to 0.6 eV as the dominating ionic conduction mechanism for the Li-Si-O ternary system. Such a result indicates these Li-Si-O phases may play an important role in achieving fast electrode kinetics, which is advantageous not only as high-rate anodes, but also as protection layer for stable lithium metal anodes. These results will play an indispensable role in computational materials design for both lithium-ion and lithium-metal batteries.

2. Results and Discussion

Before structure prediction, we determined 34 Li: Si: O ratios by the valence balance principle primarily, and then applied CALYPSO to predict the Li-Si-O phases according to these ratios. On the basis of predicting ideal structures, VASP was applied to analyze the stability of these predicted structures and screen out the stable new phases. Finally, the physicochemical properties of these new phases were analyzed by VASP, and their electrochemical properties were studied. Figure 1a presents the exploration process of the Li-Si-O ternary system and a variety of software were applied to collaboratively study the properties of the Li-Si-O ternary system.

2.1 Structure prediction

Using an unbiased swarm-intelligence structure searching method, we identified stable structures in the Li-Si-O ternary system. The difficulty in the prediction of ternary system lies in the high complexity of the space group and the variety of element ratios. Therefore, a new strategy based on valence analysis is proposed to make preliminary judgments on the rationality of the composition to be searched over. It is believed that different elements in a covalent-type compound form stable covalent bonds by sharing electron pairs with each other. Thus, they exhibit different valences. In the Li-Si-O system, the common valence of Si atom varies from -4 to +4, the common valence state of O atom varies from -2 to -1, and the valence state of Li atom is in general +1. Herein, we combine these different valence states to discover all possible chemical ratios that meet the requirement on electron balance (when the summation of the valences is zero), which is also satisfied by the existent phases including $Li_2Si_2O_5$, Li_2SiO_3 and Li_4SiO_4. 34 combinations are identified after quick iteration over all possibilities, which is listed

in Table S1. After that, structure prediction on a large number of compositions is carried out. 34 compounds with lowest relative formation energy were screened out. In Table S1, we list all the predicted chemical ratios as well as their most stable crystal structures and lattice parameters. The lithium content is between 7.1% (for $LiSi_5O_8$) and 70% (for Li_7SiO_3). The P1 space group occurs most frequently among these low energy phases (13 out of 34).

The formation energy and energy-above-hull are calculated for the newly discovered phases. The formation energy is calculated by subtracting the total energy of the atoms from the compound's total free energy. The specific formula is shown as follows:

$$E_{\text{formation}} = \frac{E(\text{Li}_x\text{Si}_y\text{O}_z) - x \cdot E(\text{Li}) - y \cdot E(\text{Si}) - z \cdot E(\text{O})}{x+y+z} \quad (1)$$

Chemical potentials of lithium, silicon and oxygen are all calculated based on the solid structure from the Materials Project database. After obtaining the formation energy of all predicted phases, we calculated the energy-above-hull (E_{hull}, the formation energy difference between a phase and its adjacent phases) to determine the stability of predicted phases. Sorted by E_{hull}, all the structures can be classified into four types: stable, almost stable, metastable, and unstable phases, respectively. When the energy locates below the hull, the formation energy of the specified phase is lower than that of all adjacent phases in the phase diagram, and such a phase is considered thermodynamically stable. Table S1 shows that the most stable phases are Li_4SiO_6, Li_2SiO_5, and Li_4SiO_8 whose lithium content are 36.4%, 25%, and 30.8%, respectively. When the phase's E_{hull} is positive but smaller than 0.1 eV/atom, it has a high probability

to form considering the entropy effect as well the effect of chemical potential of other elements [49]. Therefore, they are viewed as almost-stable phases. If the E_{hull} is between 0.1 eV/atom and 0.2 eV/atom, they are metastable. An E_{hull} greater than 0.2 eV/atom can induce the unstable phases accordingly. Figure 1b shows the relationship between valence of silicon in the compound and E_{hull}. When the valence of silicon equals to +4 and −1, the corresponding structure tends to be more stable. Among the two compounds known to exist stably in nature, SiO_2 and LiSi, Si exhibits +4 and -1 valences, respectively. While in the stable Li-Si-O systems we predicted, Si also exhibits these two valences, which demonstrates that the formation of Si-O and Li-Si bonds can stabilize the Li-Si-O structure to a certain degree. Such bonds are also the dominant binding mode in the existing Li-Si-O compounds.

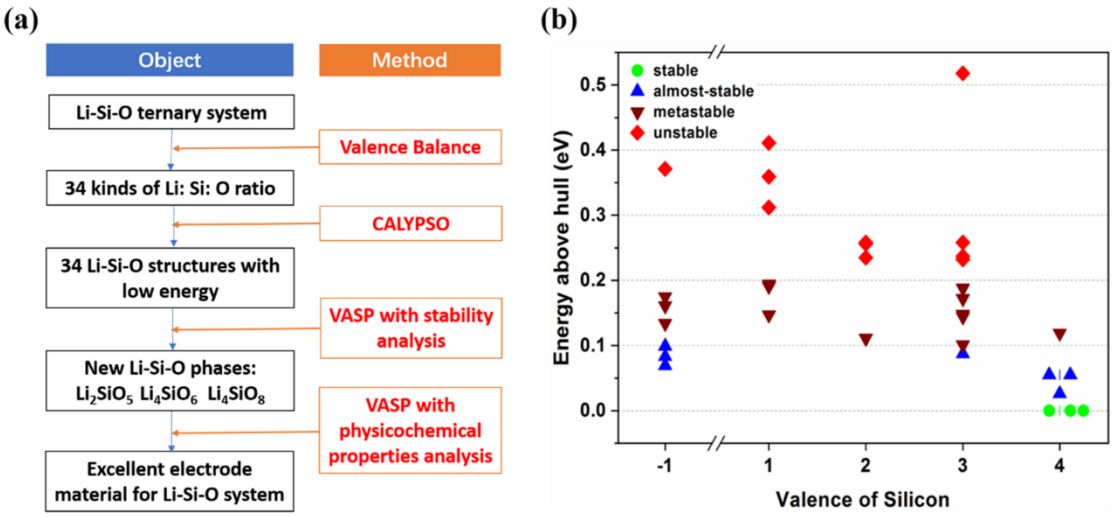

Figure 1. (a) Schematic diagram of the screening process for Li-Si-O ternary system. (b) The relationship between energy-above-hull and the valence of silicon. The green, blue, brown, and red dots represent the stable, almost-stable, metastable, and unstable phases, respectively.

We further focus on the three new thermodynamically stable phases Li_2SiO_5, Li_4SiO_6 and Li_4SiO_8 located on the hull. The detailed parameters of these crystalline

phases are listed in Table 1. Herein, phase diagrams are constructed to show their thermodynamic phase equilibria of multicomponent systems. Based on the Materials Project database, we added the three new phases to the phase diagram of Li-Si-O by referring to the energy of all known phases, as shown in Figure 2. Among them, Li_4SiO_6 possesses the highest lithium concentration (Figure 2b). According to the position of the three new phases in the phase diagram, all surrounding phases are possible decomposition products during the lithium insertion/extraction processes, and can be predicted. For example, the adjacent phases of Li_4SiO_6 are Li_2SiO_3, Li_4SiO_4, and Li_2O_2, which indicates that Li_4SiO_6 could form via a four-phase coexistence reaction or it can decompose into these adjacent phases.

Table 1. Structural details of the three new stable phases.

Formula	Formation energy (eV/Atom)	Space group	Lattice parameters (Å, deg)
Li_4SiO_6	-1.303	P1(1)	a = 2.91, b = 5.85, c = 5.48 α = 77.7, β = 89.9, γ = 104.4
Li_2SiO_5	-1.591	P1(1)	a = 5.02, b = 5.07, c = 5.63 α = 110.2, β = 67.8, γ = 115.6
Li_4SiO_8	-1.552	P1(1)	a = 4.95, b = 5.03, c = 6.42 α = 92.5, β = 94.3, γ = 117.8

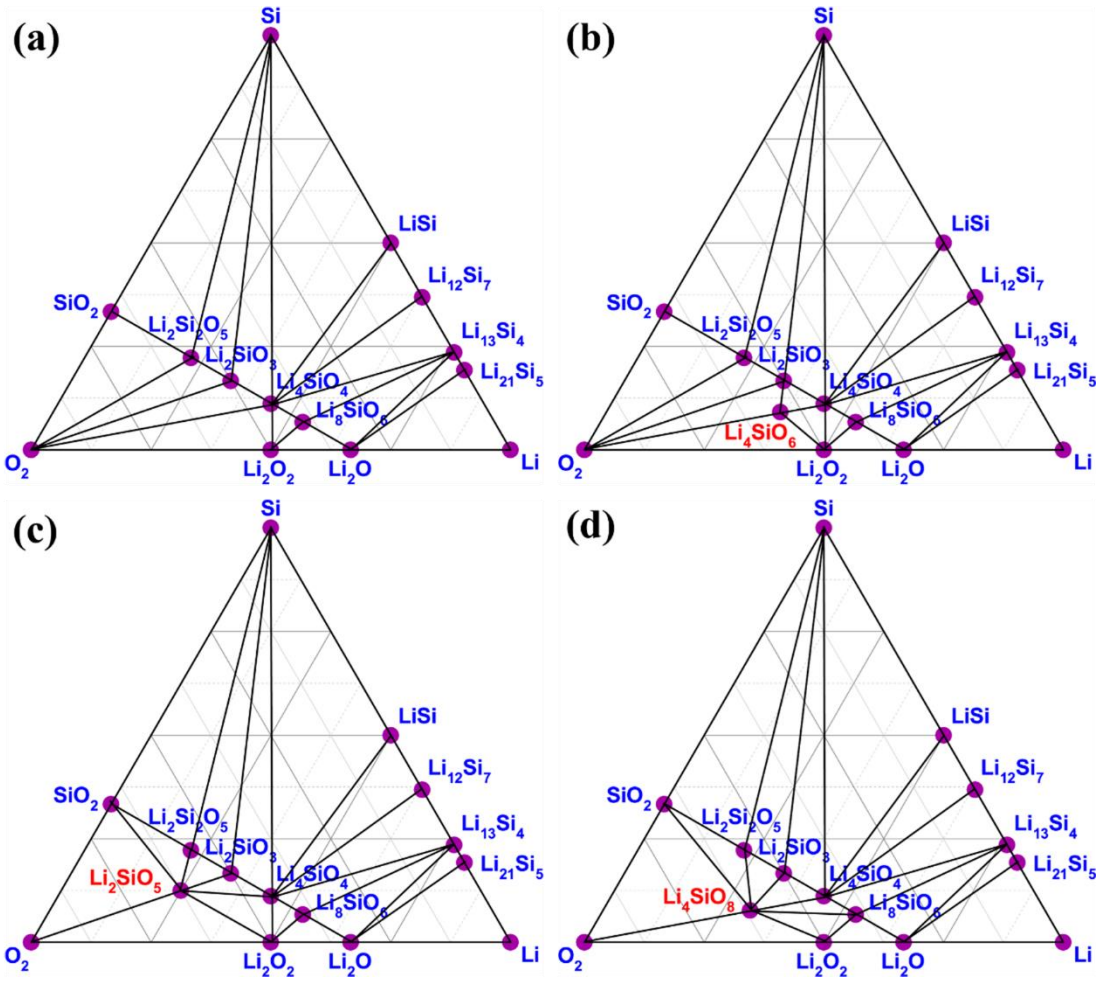

Figure 2. Ternary Li-Si-O_2 phase diagrams for (a) original phase diagram from Materials Project database, (b) new phase diagram with Li_4SiO_6 as comprised to the database, (c) new phase diagram with Li_2SiO_5, (d) new phase diagram with Li_4SiO_8.

Figure 3 exhibits the atomic structure of the three new phases. Their crystal structures are more complex than the known ones, with the lowest symmetry and belong to the P(1) space group. To further confirm the stability of these predicted structure, we computed the phonon spectra of three phases (Figure S1). It can be seen that there is almost no imaginary frequency, which theoretically proves their dynamic stability. Furthermore, these structures are not densely packed. Accordingly, large interspace exists. Such geometric characteristics are potentially helpful for fast diffusion of Li ions, which we will look at in section 2.2.

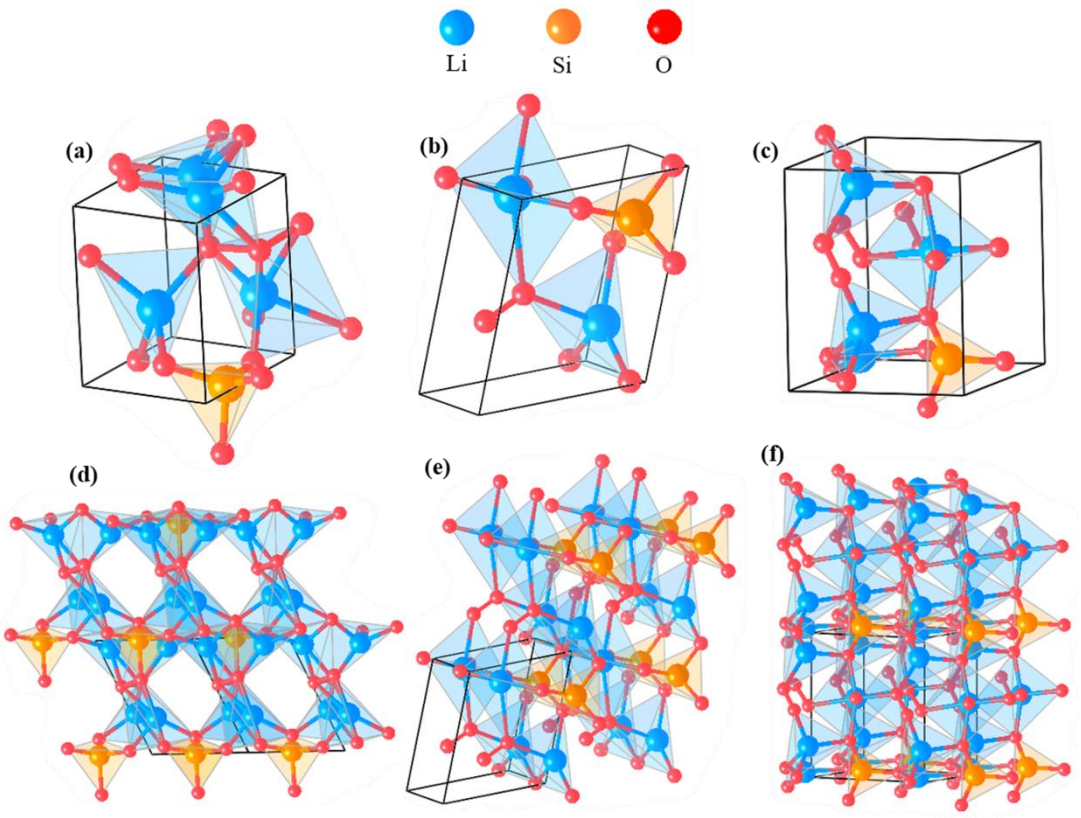

Figure 3. Structure of the three new stable phases for (a) primitive cell of Li_4SiO_6, (b) primitive cell of Li_2SiO_5, (c) primitive cell of Li_4SiO_8, (d) 2×2×2 supercell of Li_4SiO_6, (e) 2×2×2 supercell cell of Li_2SiO_5, (f) 2×2×2 supercell of Li_4SiO_8.

2.2 Physicochemical properties on new phases predicted via first-principles

Next, the electronic structure of Li-Si-O system was investigated. The electronic structure is critical in determining the electron mobility and will influence the rate capability of the electrode by affecting the electron transport. We further calculated the total density of states (DOS) of three new phases, *i.e.*, Li_4SiO_6, Li_2SiO_5 and Li_4SiO_8. As shown in Figure 4(b), Li_4SiO_6 exhibits insulator feature with an energy gap of ~ 4 eV, while Li_2SiO_5 and Li_4SiO_8 are conductive as indicated by the non-zero DOS at Fermi level (Figure 4a and 4c). These results suggest that the Li-Si-O ternary compounds can serves as protection layers for lithium metal anode [44] or electrode materials for lithium-ion batteries. For lithium-metal anode protection, Li_4SiO_6 is

anticipated to have low electrical conductivity and excellent stability against electrolyte environment. For electrode applications, Li_2SiO_5 and Li_4SiO_8 have good electrical conductivity and high lithium storage capacity. All the three materials have excellent Li-ion transport properties (Figure 5). Moreover, all three predicted phases do not exhibit magnetic features. In brief, from the electronic structures of the predicted phases, it can be seen that the discovery of new predicted phases complements the electrochemical properties of the entire Li-Si-O system, demonstrating that the Li-Si-O ternary system has a broad prospect as a battery material.

During the electrochemical reactions, the lithium potential has significant effect on the phase stability of materials with different lithium content. In order to better evaluate the stability of compounds during the charge and discharge processes, we calculated the electrochemical stability window for different phases. In Figure 4(d), three known phases (the green column) inquired from database were also calculated to compare with the predictive phases (the blue column). The stability window of the three predictive phases is relatively narrow, and has a high stability potential against lithium metal (ranging from 4.8 to 5.8 V). The electrochemical stability windows of predicted phases are relatively narrow and thus it is speculated that these predicted phases may appear as intermediate states during Li stripping/plating processes. However, the discovery of the new phases widens the electrochemical stability window of the entire Li-Si-O system, ensuring that various stable Li-Si-O structures can exist in a large voltage range during Li stripping/plating processes and guaranteeing the stability of the system. In brief, the wide electrochemical window of the entire Li-Si-O ternary system

demonstrates that the Li-Si-O ternary system still can be applied as superior electrode materials and the predicted phases we discovered may emerge as intermediates during the charging/discharging process.

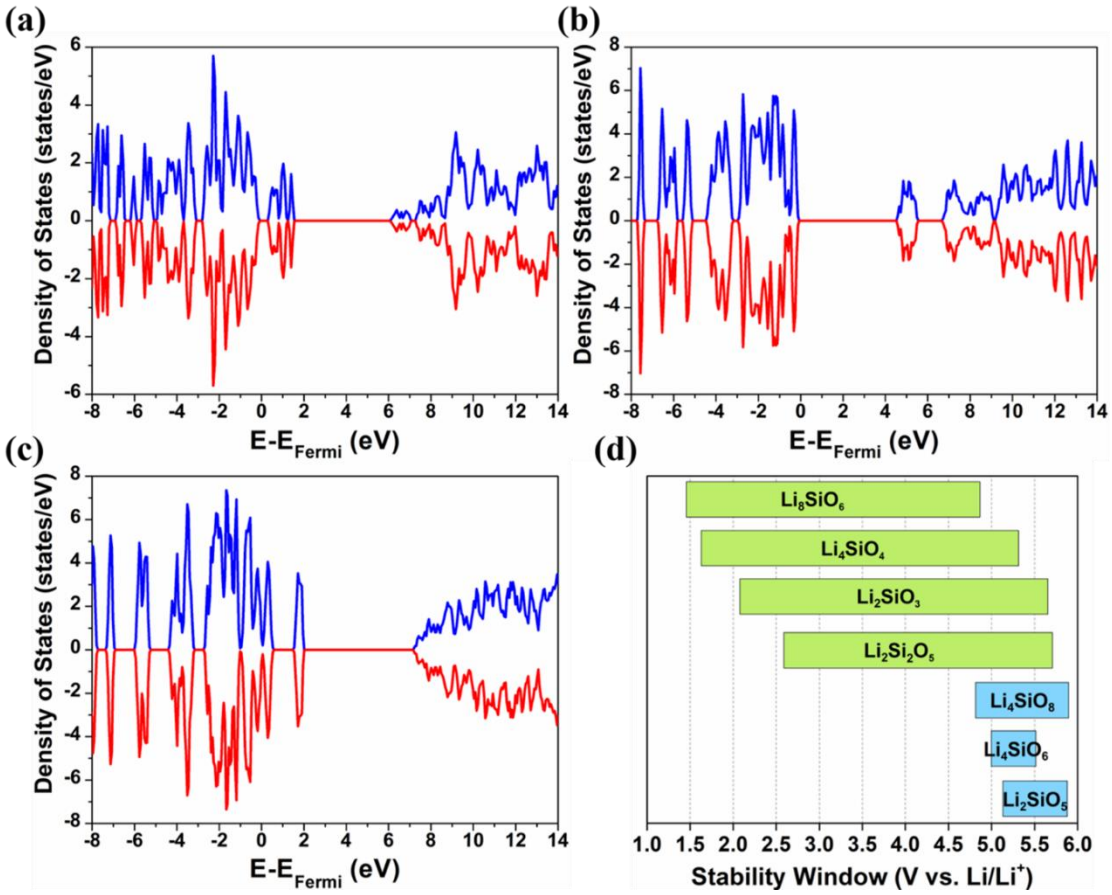

Figure 4. Total DOS of (a) Li_2SiO_5, (b) Li_4SiO_6 and (c) Li_4SiO_8. (d) Electrochemical stability windows of predicted phases (blue) and known phases (green). The phases in the stability window range are stable as the chemical potential of lithium changes.

The mechanical properties of Li-Si-O ternary alloy systems play an important role in describing the resistance of material against mechanical deformation [50] and can be roughly estimated by the elastic constants. We calculated the independent elastic stiffness constants (C_{ij}) and compliance constants (S_{ij}) for the three Li-Si-O phases, and listed the simulation results as per Table S2. These independent elastic constants are found to satisfy the Born stability criteria for crystal [50,51], expressed by $C_{11} > 0$; $C_{33} >$

0; $C_{44} > 0$; $C_{66} > 0$; $C_{11}-C_{12} > 0$; $C_{11}+C_{33}-2C_{13} > 0$; $2(C_{11}+C_{12}) + C_{33} + 4C_{13} > 0$, implying their well mechanical stability. The mechanical strength of Li-Si-O phases were estimated by their elastic modulus obtained from the elastic stiffness constants [52]. Table 2 presents the Young's moduli, the shear moduli and the bulk moduli of Li-Si-O ternary alloy systems and conventional Li-Si binary alloy systems. The moduli of the predicted phases (Li_2SiO_5, Li_4SiO_6 and Li_4SiO_8) are lower than those of the known phases ($Li_2Si_2O_5$, Li_2SiO_3 and Li_4SiO_4). However, the mechanical strength of the predicted phases is much better than that of lithium metal (*e.g.,* 76.8, 86.6, 65.9 GPa *vs.* 15.2 GPa in Young's moduli). According to the linear perturbation model by Monroe and Newman, such high shear moduli could block the penetration of lithium dendrites and stabilize the lithium metal anode in lithium-metal batteries [53]. In fact, compared with the traditional Li-Si binary alloy systems, the Li-Si-O ternary alloy electrode also exhibits advantages in bulk moduli, reflecting superior resistance against mechanical deformation during Li stripping/plating processes.

Table 2. Young's moduli (E), shear moduli (G), and bulk moduli (K) of Li-Si-O ternary alloy systems and other conventional Li-Si binary alloy systems.

Compound	E: Young's Moduli (GPa)	G: Shear moduli (GPa)	K: Bulk moduli (GPa)
Li_2SiO_5	76.8	30.7	62.9
Li_4SiO_6	86.6	35.2	60.8
Li_4SiO_8	65.9	26.6	45.4
$Li_2Si_2O_5$	123.3	50.4	76.5
Li_2SiO_3	126.4	52.7	74.6
Li_4SiO_4	107.6	43.5	70.6
Li	15.2	6.1	12.3

$Li_{13}Si_4$	65.4	28.2	33.1
$Li_{12}Si_7$	73.2	33.2	36.4
$Li_{21}Si_5$	61.4	26.6	30.5
Li_7Si_3	74.3	32.5	36.4
LiSi	84.1	36.1	52.2

The excellent ionic conductivity can accelerate the lithiation reactions, allowing the lithium ions on the surface of anodes to transport into the bulk in time to avoid uneven deposition of lithium at high current densities, thereby preventing the formation of lithium dendrites [46]. The migration barriers of ions are jointly determined by the Li(s)-host electron interaction and the Coulomb repulsion of cations. Herein, transition states are identified using first-principles based CI-NEB method to evaluate the Li-ion conductivity of the three new phases. The transport of lithium ions in crystals can be divided into two types: interstitial-mediated diffusion and the vacancy-mediated counterpart. Interstitial-mediated diffusion refers to the hop of free ions between the gaps inside the crystal, while vacancy-mediated diffusion refers to the process in which ions of the material itself are separated from their original positions and enter the adjacent gap. Before evaluating the barrier, potentially stable sites were explored to identify the reasonable long-term pathway for Li-ion diffusion. Due to the complexity of the structures and the low spatial symmetry, many inequivalent stable/metastable sites for intercalated lithium are existent. In order to exhaust all of the intercalated conformation, we sampled initial configurations by rationally generating interstitial sites according to the interspace distribution. We developed a scoring method to determine whether an interstitial site is suitable as the initial diffusion state. The scoring

function can be expressed as:

$$\text{Score} = \frac{1}{n}\sum_n d(R) + \frac{1}{S^2(\bar{d})} \quad (2)$$

where $d(R)$ is the distance between an atom in interstitial site and a surrounding atom, and $S^2(\bar{d})$ represents the variance of the average distance. A higher score indicates a higher probability as an interstitial site. Using the scoring function, we efficiently screened out all of the stable or metastable states in the crystal. For each pairs of neighboring intermediate state, we created a number of intermediate states by linear interpolation on the diffusion pathway, and calculated the activation barrier by CI-NEB method. For comparison, we also selected three known phases and calculated their Li-ion conductivity using the same method.

Figure 5 shows the energy barrier of the Li hops via interstitial-mediated diffusion and vacancy-mediated diffusion in different Li-Si-O ternary phases. For each phase, we found 2-3 non-equivalent diffusion pathways based on which the Li ions can realize long-range transport in the crystal. Clearly, the lithium conductivity is anisotropic. For interstitial diffusion, the energy barriers along different directions are significantly different, ranging from 0.3 eV to 0.9 eV in Li_4SiO_6 as shown in Figure 5(a). Similarly, the energy barriers of Li_2SiO_5 (Figure 5(b)) and Li_4SiO_8 (Figure 5(c)) are also different in different directions (0.1~0.7 eV in Li_2SiO_5 and 0.6~1.1 eV in Li_4SiO_8). Such strong anisotropic effect can be attributed to the uneven distribution of interspace among on-site atoms, while the fast diffusion channel for Li-ion diffusion exists in specific orientation, within which the lithium transport can be less obstructed by host atoms (illustrations in Figure 5). In all three new phases, there exists fast diffusion channels

with the diffusion barrier below 0.6 eV, which is comparative to or smaller than the three known phases (Figure 5d, 5e, 5f for $Li_2Si_2O_5$, Li_2SiO_3, Li_4SiO_4). With such low energy barriers, long-range diffusion of lithium ions can happen rapidly. Table 3 lists the diffusion rate calculated from the energy barrier. The diffusivity of predicted phases is potentially superior to the known phases. Compared with the existing phases, the Li-ion diffusion rates the predicted phases in some directions are still comparable (4.523×10^{-6} $cm^2\cdot S^{-1}$ in Li_2SiO_5 vs. 6.188×10^{-6} $cm^2\cdot S^{-1}$ in $Li_2Si_2O_5$ and 3.926×10^{-8} $cm^2\cdot S^{-1}$ in Li_2SiO_3, 1.602×10^{-9} $cm^2\cdot S^{-1}$ in Li_4SiO_4). Compared with the Li-ion diffusion rates in other electrode materials, the diffusion rate of lithium ions in the Li-Si-O phase is also comparable (4.523×10^{-6} $cm^2\cdot S^{-1}$ in Li_2SiO_5, 6.188×10^{-6} $cm^2\cdot S^{-1}$ in $Li_2Si_2O_5$ vs. $\sim10^{-6}$ $cm^2\cdot S^{-1}$ on graphene [54] and $\sim10^{-12}$ $cm^2\cdot S^{-1}$ in rutile [55], $\sim10^{-7}$ $cm^2\cdot S^{-1}$ in Si [56], $\sim10^{-7}$ $cm^2\cdot S^{-14}$ in diamond [57]), which indicate the excellent lithium-ion transport performance in Li-Si-O phase. Among them, Li_2SiO_5 has the lowest energy barrier of about 0.1 eV, indicating that these predicted phases play a competitive role on promoting the charging rate of the battery.

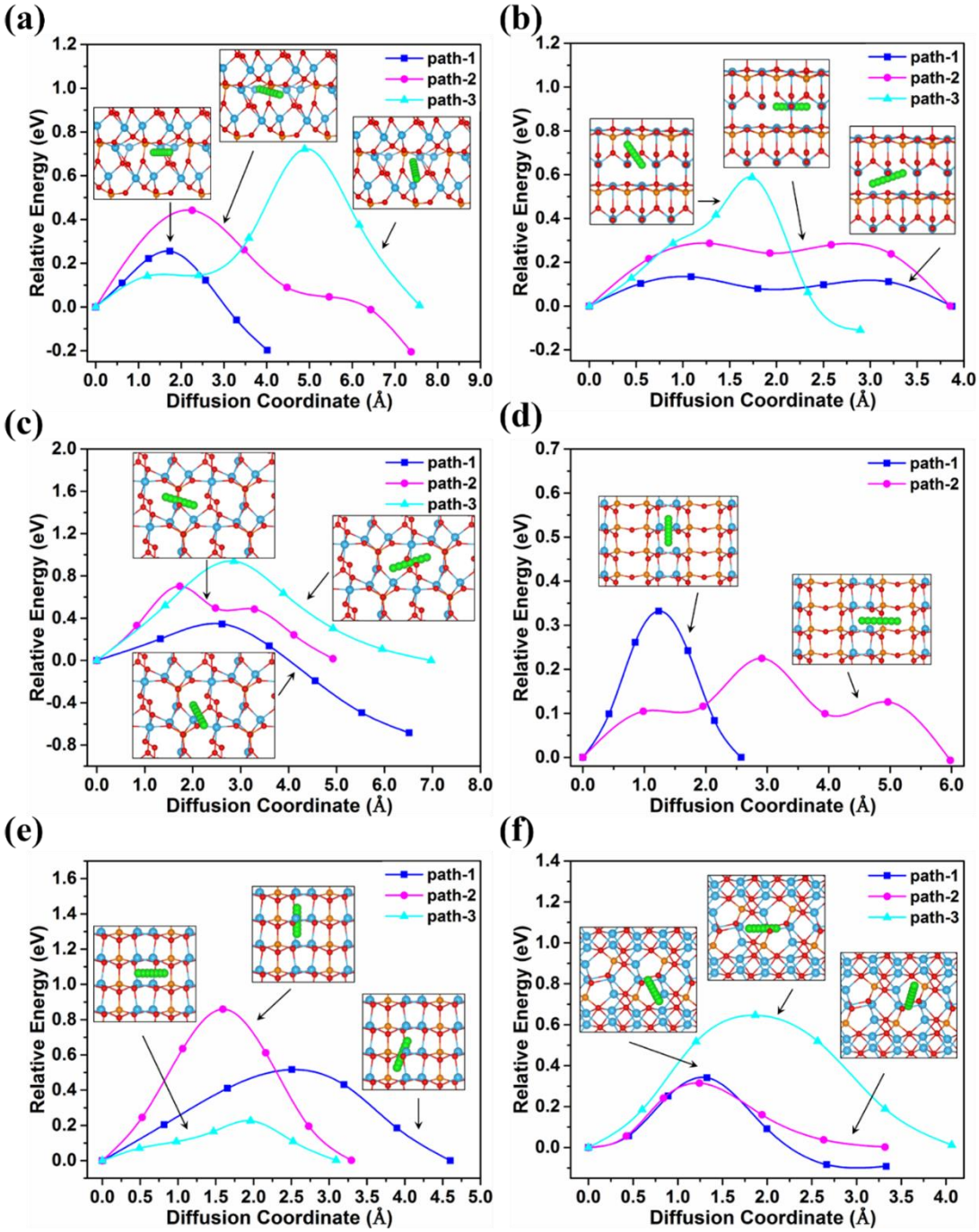

Figure 5. Interstitial diffusion along different path of new predicted phases for (a) Li_4SiO_6, (b) Li_2SiO_5, (c) Li_4SiO_8, and known phases from Materials Project database for (d) $Li_2Si_2O_5$, (e) Li_2SiO_3, (f) Li_4SiO_4. Illustration shows the stable initial and final interstitial structures and diffusion paths.

Table 3. Diffusion rate for Li^+ ion diffusion through the predicted phases and known phases at room temperature (300 K).

Diffusion path	Diffusion rate ($cm^2 \cdot S^{-1}$)					
	Li_4SiO_6	Li_2SiO_5	Li_4SiO_8	$Li_2Si_2O_5$	Li_2SiO_3	Li_4SiO_4
Path1	1.139×10^{-11}	4.523×10^{-6}	5.765×10^{-21}	9.035×10^{-9}	1.165×10^{-12}	1.936×10^{-11}
Path2	1.360×10^{-14}	5.359×10^{-9}	1.535×10^{-12}	6.188×10^{-8}	1.896×10^{-18}	1.602×10^{-9}
Path3	8.029×10^{-16}	7.602×10^{-16}	1.843×10^{-19}	/	3.926×10^{-8}	7.56×10^{-15}

The Li transport properties via the vacancy-mediated route are also systematically investigated. The migration barriers for various pathways are shown in Figure S2. We found that the anisotropic effect for Li vacancy diffusion is even stronger than that of its interstitial counterpart, with the energy differences varying from 0.1 eV to 1.4 eV. However, the mechanism of such anisotropic effect of vacancy diffusion is quite different from the interstitial diffusion. The complex structures and coordination environments inside Li-Si-O ternary compounds result in different energies for lithium ions at different positions to detach from the host, which is the origin of anisotropic effect in vacancy diffusion. According to the comparison of migration barriers between interstitial diffusion and vacancy diffusion in the same phase, it clearly shows that the energy barrier of interstitial diffusion is generally lower. For the long-term diffusion process, Li hopping through the bottleneck with the highest energy barrier along the fastest channel becomes the rate limiting step which determines the diffusivity. As a result, the probability of interstitial diffusion is much higher than vacancy diffusion, which can be viewed as the dominant diffusion mechanism in Li-Si-O material system. Such diffusion trend can be primarily attributed to the strong Li-O ionic bond and Si-O covalent bond, while the energy cost for lithium atom to leave its original position in

host will be very high, thus reducing the possibility of free Li-ions squeezing out the host atoms. In addition, the high energy cost can also induce low defect concentration, which will further shrink the feasibility for vacancy diffusion.

Conclusion

In summary, we carried out crystal structure predictions on the Li-Si-O ternary system. Valence analysis and formation energy computations are performed to verify the rationality and stability of these predicted phases. Three new stable phases which have the potential to be applied as alloy anodes for lithium-ion batteries were theoretically identified. The analysis on valence and energy indicates that the new phases are more possible to be thermodynamically stable based on the basic valence to elements. DOS analysis further shows that these new phases can serve as promising electrode or protection layers on the anode side. By comparing with the known phases ($Li_2Si_2O_5$, Li_2SiO_3, Li_4SiO_4), high Li diffusivity is predicted in the new phases. Moreover, these new phases complement the phase transition processes of the electrode during charge and discharge. These findings provide important insight towards the rational design of ternary electrode materials and guide future discovery of other ternary systems.

Acknowledgements

Q. F. Z. was supported by the Beijing Natural Science Foundation (2192029), the National Key Research and Development Program of China (2017YFB0702100), the National Natural Science Foundation of China (11404017, 12004145), the Technology Foundation for Selected Overseas Chinese Scholars, and the Ministry of Human

Resources and Social Security of China. J. L. Q. was supported by the Academic Excellence Foundation of BUAA for PhD Students. Z. L. is supported by the Faraday Institution (grant number FIRG017). Z. W. S. is supported by the Singapore National Research Foundation (NRF-NRFF2017-04). B. L. is supported by Jiangxi Provincial Natural Science Foundation (20212BAB214032).

Conflict of Interest

The authors declare no conflict of interest.

Keywords

lithium metal battery; alloy anodes; structure prediction; electrical properties; first-principles calculations

Reference

[1] J. B. Goodenough, H. D. Abruna, M. V. Buchanan, *Electric Batteries*. **2007**, 4, 186.

[2] B. Dunn, H. Kamath, J. M. Tarascon, *Science*. **2011**, 334(6058):928–935.

[3] J. W. Choi, D. Aurbach, *Nature Reviews Materials*. **2016**, 1(4):16013–16028.

[4] M. Yoshio, H. Y. Wang, K. Fukuda, Y. Hara, Y. Adachi, *Journal of the Electrochemical Society*, **2000**, 147:1245–1250.

[5] W. Xu, J. Wang, F. Ding, *Energy & Environmental Science*, **2014**, 7(2):513–537.

[6] K. Hansu, J. Goojin, U. K. Young, *Chemical Society Reviews*, **2013**, 42(23):9011–9034.

[7] L. Ziheng, S. Fan, E. M. Yue, *Journal of Energy Chemistry*, **2020**, 58, 170.

[8] C. Jiahua, Y. Zheng, L. Guohua, *Energy Storage Materials*, **2020**, 25:305–312.

[9] Z. Lu, F. Ciucci, *Chemistry of Materials*, **2017**, 29(21): 9308–9319.

[10] D. Aurbach, E. Zinigrad, H. Teller, P. Dan, *Journal of the Electrochemical Society*, **2000**, 147:1274–1279.

[11] J. F. Qian, A. Wesley, Henderson, X. Wu, *Nature Communications*, **2015**, 6:6362–6370.

[12] Z. Lu, J. Liu, F. Ciucci, *Energy Storage Materials*, **2020**, 28:146–152.

[13] H. R. Jiang, Z. Lu, M. C. Wu, *Nano Energy*, **2016**, 26, 97–104.

[14] L. Ziheng, Y. Jing, W. Junxiong, *Energy Storage Materials*, **2019**, 18:311–319.

[15] T. Wang, J. Qu, D. Legut, *Nano Letters*, **2019**, 19: 3122–3130.

[16] Q. Huang, S. Ni, M. Jiao, X. Zhong, G. M. Zhou, H. M. Cheng, *Small*, 2021, 17, 2007676.

[17] H. Deng, F. Qiu, X. Li, *Electrochemistry Communications*, **2017**, 78:11-15.

[18] M. N. Obrovac, V. L. Chevrier, *Chemical Reviews*, **2014**, 114(23):11444-11502.

[19] M. T. Mcdowell, S. W. Lee, W. D. Nix, *Advanced Materials*, **2013**, 25(36):4966-4985.

[20] B. Fuchsbichler, C. Stangl, H. Kren, *Journal of Power Sources*, **2011**, 196(5):2889-2892.

[21] V. Manev, I. Naidenov, B. Puresheva, *Journal of Power Sources*, **1995**, 55(2):211-215.

[22] K. L. Lee, J. Y. Jung, S. W. Lee, *Journal of Power Sources*, **2004**, 129(2):270-274.

[23] B. Philipp, J. Sebastian, Z. Klaus, *Cheminform*, **2014**, 45(4):1-2.

[24] X. Wang, R. Xiao, H. Li, *Physical Review Letters*, **2017**, 118(19):195901.

[25] S. P. Ong, Y. Mo, W. D. Richards, *Energy & Environmental Science*, **2012**, 6.148-156.

[26] N. Kamaya, K. Homma, Y. Yamakawa, *Nature Materials*, **2011**, 10(9):682-686.

[27] A. M. Nolan, Y. Zhu, X. He, Q. Bai, Y. Mo, *Joule* 2018, 2, 2016-2046.

[28] R. Murugan, V. Thangadurai, W. Weppner, *Angewandte Chemie International Edition*, **2010**, 46(41):7778-7781.

[29] K. L. Lee, J. Y. Jung, S. W. Lee, *Journal of Power Sources*, **2004**, 129(2):270-274.

[30] C. H. Doh, C. W. Park, H. M. Shin, *Journal of Power Sources*, *2008*, 179(1):367-370.

[31] A. Netz, R. A. Huggins, W. Weppner, *Journal of Power Sources*, **2003**, 119(1):95-100.

[32] W. J. Weydanz, M. Wohlfahrtmehrens, R. A. Huggins, *Journal of Power Sources*, **1999**, 81(9):237-242.

[33] S. Wang, Q. Bai, A. M. Nolan, *Angewandte Chemie International Edition*, **2019**. 58(24):8039-8043.

[34] B. Chen, T. Wang, S. Zhao, J. Tan, N. Zhao, S. Jiang, Q. Zhang, G. M. Zhou, H. M. Cheng, *Advanced Materials*, 2021, 33: 2007090.

[35] Z. Han, S. Zhao, J. Xiao, X. Zhong, J. Sheng, W. Lv, Q. Zhang, G. M. Zhou, H. M. Cheng, *Advanced Materials*, 2021, 33: 2105947

[36] J.O. Besenhard, *Wiley-VCH*, **2011**. F. Walsh, J.O. Besenhard, *Journal of*

Applied Electrochemistry, **1999**, 29(9):1139-1139. 10.1023/A:1003858328924

[37] R. A. Huggins, *Solid State Ionics, Diffusion & Reactions*, **1998**, 113(115):57-67.

[38] J. Schoonman, R. A. Huggins, *Journal of Solid State Chemistry*, **1976**, 16(3):413-422.

[39] R. A. Sharma, R. N. Seefurth, *Chemischer Informationsdienst*, **1977**, 8(11):1-2.

[40] M. M. O. Thotiyl, S. A. Freunberger, Z. Peng, *Nature Materials*, **2013**, 12(11):1050-1056.

[41] Y. Chen, S. A. Freunberger, Z. Peng, *Nature Chemistry*, **2013**, 5(6):489-494.

[42] Z. Peng, S. A. Freunberger, Y. Chen, *Science*, **2012**, 337(6094):563-566.

[43] B. D. Adams, C. Radtke, R. Black, *Energy & Environmental Science*, **2013**, 6(6):1772.

[44] D. Lin, J. Zhao, J. Sun, *Proceedings of the National Academy of Sciences of the United States of America*, **2017**, 114(18):4613-4618.

[45] G. Hautier, A. Jain, H. Chen, *Journal of Materials Chemistry*, **2011**, 21(43):17147.

[46] S. M. Ying, A. D. Dompablo, *Energy & Environmental Science*, **2009**, 2(6):589-609.

[47] A. Urban, D. H. Seo, G. Ceder, *Npj Computational Mathematics*, **2016**, 2(1):16010-16022.

[48] B. He, S. Chi, A. Ye, *Scientific Data*. **2020,** 7(151):1-13.

[49] W. Sun, S. T. Dacek, S. P. Ong, G. Hautier, A. Jain, W. D. Richards, A. C. Gamst, K. A. Persson, G. Ceder, *Science Advances*, **2016**, 2(11):160225-160232.

[50] C. J. Yu, U. S. Hwang, Y. C. Pak, *New Journal of Chemistry*. **2020**, 7 (24): 1-9.

[51] M. Born, H. Kun, *Dynamical Theory of Crystal Lattices,* Clarendon, Oxford, UK, **1956**.

[52] S. H. Zhang, R. F. Zhang, *Computer Physics Communications*, **2017**, 220: 403-416.

[53] C. Monroe, J. Newman, *Journal of The Electrochemical Society,* **2003**, 150 (10): 1377-1384.

[54] K. Zhong, Y. Yang, G. Xu, J. M. Zhang, Z. Huang, *Materials*, **2017**, 10(7): 761.

[55] M. V. Koudriachova, N. M. Harrison, S. Leeuw, *Solid State Ionics*, **2003**, 157(4): 35-38.

[56] B. I. Boltaks, in: Diffusion in Semiconductors, Ed. H. J. Goldsmid, Infosearch Ltd. London,**1963**.

[57] C. U. Saguy, C. Cytermann, B. Fizgeer, V. Richter, R. Brener, R. Kalish, *Physica Status Solidi,* **2002**,193(3): 508-516.

Table of Contents

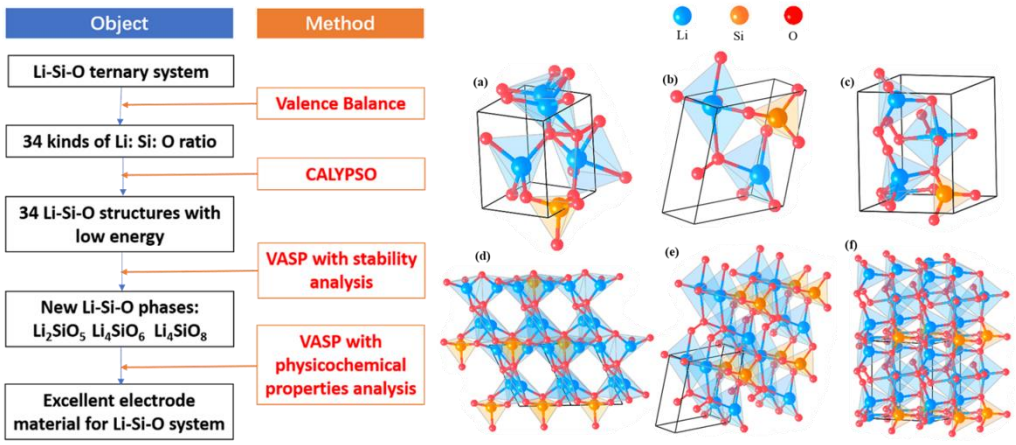

Applying high-throughput crystal structure prediction to predict Li-Si-O ternary system. Three new stable phases which have the potential to be applied as alloy anodes for lithium-ion batteries were theoretically identified. The discovery of new predicted

phases complements the electrochemical properties of the entire Li-Si-O system, demonstrating that the Li-Si-O ternary system has a broad prospect as a battery material.